CrossMark

ORIGINAL

Study of high viscous multiphase phase flow in a horizontal pipe

Yahaya D. Baba[1,2] · Aliyu M. Aliyu[3] · Archibong-Eso Archibong[1,3,] ·
Almabrok A. Almabrok[4] · A. I. Igbafe[2]

Abstract Heavy oil accounts for a major portion of the world's total oil reserves. Its production and transportation through pipelines is beset with great challenges due to its highly viscous nature. This paper studies the effects of high viscosity on heavy oil two-phase flow characteristics such as pressure gradient, liquid holdup, slug liquid holdup, slug frequency and slug liquid holdup using an advanced instrumentation (i.e. Electrical Capacitance Tomography). Experiments were conducted in a horizontal flow loop with a pipe internal diameter (ID) of 0.0762 m; larger than most reported in the open literature for heavy oil flow. Mineral oil of 1.0–5.0 Pa.s viscosity range and compressed air were used as the liquid and gas phases respectively. Pressure gradient (measured by means differential pressure transducers) and mean liquid holdup was observed to increase as viscosity of oil is increased. Obtained results also revealed that increase in liquid viscosity has significant effects on flow pattern and slug flow features.

✉ Yahaya D. Baba
   y.baba9550@gmail.com

1   Oil and Gas Engineering Centre, Cranfield University, Cranfield, UK

2   Chemical/Petroleum Engineering Department, Afe Babalola University, PMB 5454, Ado-Ekiti, Nigeria

3   School of Mechanical Engineering, Pusan National University, 609-735 Busan, Republic of Korea

4   Department of Petroleum Engineering, Faculty of Engineering, Sirte University, Sirte, Libya

Nomenclature

Symbols	Denote	Units
Fr	Froude number	
g	Acceleration due to gravity	$m.\,s^{-2}$
h	Liquid height	m
L	length	m
P	Pressure	kPa
Re	Reynolds number	
V	Velocity	m/s

Greek letter

μ	Viscosity	$Pa.s$
ρ	Density	kg/m^3
γ	Shear rate	s^{-1}
σ	Surface tension	N/m

Subscripts

f	Film zone
g	Gas phase
i	interface
l	Liquid phase
m	Mixture phase
o	Oil phase
s	Superficial or slug body
t	Translational
tp	Two-phase

Acronyms

PDF	Probability Density Function
ECT	Electrical Capacitance Tomography
L/D	Length/Distance
MMTC	Multi Modal Tomography Console
$3D$	Three Dimensional
FAD	Free Air Delivery
ID	Internal Diameter
PIV	Particle Image Velocimetry
LBP	Linear Back Projection
m	Mixture phase

l	liquid
o	Oil phase
s	Superficial
g	Gas
V	Velocity

1 Introduction

1.1 Background

Heavy oil, an unconventional fossil fuel reserve is increasingly becoming important due to the rapid depletion of conventional oil reserves as the need for more energy increases. Notwithstanding, the production and transportation of such heavy oil is accompanied with difficulties owing to its viscous nature. Results from experimental studies conducted so far in literatures shows that the behaviour of high viscosity oil-gas flows differs significantly from those of low viscosity oils. This means that most of the existing prediction models in the literature developed from observations of low viscosity liquid-gas flows will not perform accurately when compared to oil-gas flow data for high viscosity oil.

Unconventional oil resources constituting heavy oil, extra-heavy oil and bitumen have been neglected in the past because of the high costs associated with its production and transportation. This is further fuelled by the inadequate understanding of the hydrodynamics of high viscous oil in pipelines credited to limited investigation involving the use of high viscous fluids. Nevertheless, heavy oil resources according to according recent investigations [1–3] constitute nearly 70% of the world's remaining oil reserves as illustrated in Fig. 1.

The multiphase flow of gas and liquid in pipeline is characterized by regimes in which phases are spatially distributed with the slug flow regime occurring over a wide range of flow condition. Intermittency is the most pertinent characteristic feature of slug flow. For high viscosity oil, slug flow schematically represented in Fig. 2 has been found by different researchers [5–8] to be the dominant flow pattern. In this flow
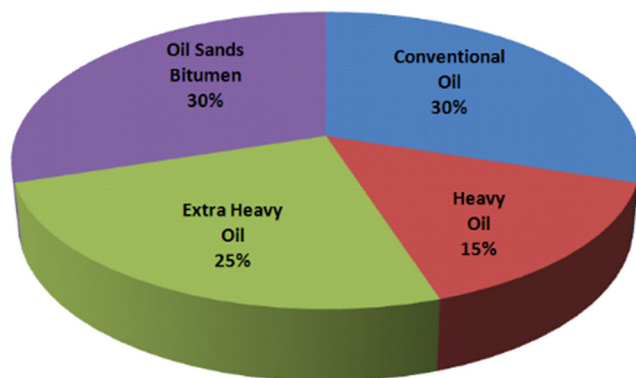
regime, liquid slugs separated by elongated gas bubbles flow intermittently through the cross-sectional area of the pipe.

A number of studies have been carried out to investigate the effects of liquid viscosity on two-phase oil-gas flows in pipelines. The pioneer study on the effects of liquid viscosity on two phase flow was conducted by [9]. The research work was carried out using 6.1 m long horizontal pipe utilizing three different diameters 0.012 m, 0.025 m and 0.051 m. Air and glycerol-water solutions with viscosities of 0.075 and 0.150 Pa.s were used as the test fluids for which different flow patterns were observed. They however concluded that the effects of liquid viscosity and surface tension were insignificant, which could be attributed to the low viscosity liquid and the length of the pipe used.

Also Nadler and Mewes, [10] conducted an experiment to investigate the effects of liquid viscosity on the phase distribution in slug flow for horizontal pipeline for liquid viscosity ranging from 0.004 to 0.037 Pa.s. Results obtained revealed that average slug liquid holdup and the elongated bubble region increased with increase in liquid viscosity.

Crowley et al., [11],Sam and Crowley, [12] studied the effects of liquid viscosity on slug flow characteristics in 0.171-m internal diameter horizontal, slightly inclined pipes. The result from their investigation for which water, glycerine-water and water-polymer solutions were used as the test fluids noted that, an increase in the liquid viscosity leads to an increase in slug velocities, liquid film heights and mean liquid holdups.

An experimental study was conducted by [13] to investigate the effects of medium viscosity oil on two phase oil-gas flow behavior in horizontal pipes. This study was carried out in a 0.0508 m-ID horizontal test pipe similar to that used by [14] for oil viscosities ranging from 0.039–0.166 Pa.s. It was noted in their investigation that the stratified smooth region shrinks as oil viscosity increases. Also noted was dispersed bubble flow, characterized by larger bubble concentration at the top of the pipe as compared with the case of low viscosity fluids.

High viscosity-oil gas flows was experimentally investigated by [15] in a 0.022 m internal diameter horizontal pipeline of 1.5 m length for oil viscosity of 0.0896 Pa.s. A flow pattern map based on their experimental data was presented. A comparison of their result with existing data for low oil viscosity oil was rather poor and thus, they highlighted the need for the development of new closure relations.

A new dataset was created by [16] based on experiment conducted using high viscous oil (0.9 Pa s) and gas in a horizontal and inclined pipe of 0.0228-m. They concluded base on their findings that discrepancies exist when experimental data for high viscosity oils are compared with those of correlations available in the literature.

Furthermore, the effects of high oil viscosity on oil/gas flow behaviour in 0.0508 m internal diameter horizontal pipeline was studied by [14] for oil viscosities ranging from

Fig. 1 Total world oil reserves -conventional versus unconventional [4]

Fig. 2 Slug Flow Geometry [4]
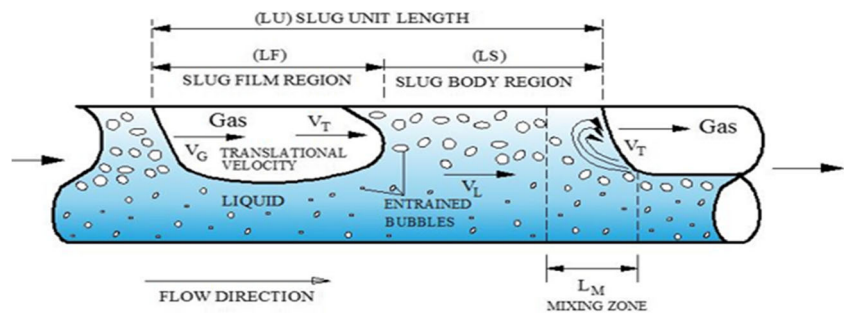
0.181–0.587 Pa.s. They noted that all flow patterns can exist for a typical gas/oil ratio within the range of flow condition investigated. Their investigation also revealed that existing mechanistic models [17, 18] tested against their data are not sufficient for high viscosity oils. Some modifications were implemented in these models resulting to better predictions of liquid holdup and pressure gradient.

More recently [4, 19] carried out modelling studies on the effects of liquid viscosity on slug flow parameters. While [4] developed a correlation for the prediction of slug frequency based on data collected using liquid viscosity ranging from 1.0–5.5 Pa.s conducted in 0.0762 m ID horizontal pipe, [19] developed a correlation for the prediction of slug length based on data collected using oil of viscosity 0.8 Pa.s in a 0.022 m ID horizontal pipe.

From the review above and others in the open literature, it is evident that the most of the existing experimental datasets for high viscous oil-gas flows are confined to liquid viscosity less than 1.0 Pa.s and mostly conducted in smaller diameter pipes.

This paper therefore presents an experimental investigation on the effects of liquid viscosity on two-phase characteristics using a non-intrusive advance instrumentation. The results presented in this research paper are from an extensive experimental campaign carried out at the Oil and Gas Engineering Centre laboratory of Cranfield University. This seeks to extend the databank and provide a clearer understanding of the physics of high viscous multiphase flows in addition to bridging the knowledge gap highlighted in the introduction above. In addition, accurate prediction of two-phase flow parameters will have significant impact on the design and specification for downstream facilities.

Electrical Capacitance Tomography (ECT) a technology that is capable of instantaneous visualisation, reconstruction and display of cross-sectional distribution of pipeline. This technology has been used in recent times for investigations and measurement of multiphase flow. ECT is a promising imaging technique with inherent potentials for multiphase flow measurement. Some of these potentials include non-invasiveness, fast imaging speed and most especially free of radiation. Investigation has shown it to be a reliable method in the measurement of non-conducting and high viscous oil and gas flows as indicated by [6, 20, 21] as against the used of other techniques such wire mesh sensors, Particle Image Volocimetry (PIV) and Laser Doppler Anemometry (LDA). While wire mesh sensors finds application in conducting fluids and are disadvantaged by their intrusive nature, optical access for the laser sheets will be the greatest limitation for PIV and LDA when used for investigating high viscous fluids. In following paragraph, a review of some investigations, which are however, limited light oil involving the application of ECT system for multiphase flow measurement is presented.

Areeba et al. [22] conducted an experimental investigation using Electrical Capacitance Tomography (ECT) technique to measure the void fraction in two phase bubble flow regime. The experiment was carried out in a vertical fluid column (ECT sensor) with internal diameter and height of 0.00493 m and 0.0409 m respectively using air and water as test fluids. Different flow regimes were established base on their findings.

Hunt et al. [23] presented a series of measurements undertaken in complex light oil/gas slug flows in a flow loop test facility of length 217 m and internal diameter of 0.069 m constructed from steel and PVC pipes. Measurement were made possible with the aid of Electrical Capacitance Tomography (ECT). 2-D cross-sectional images, time series velocity and concentration graphs and 3-D contour plots were presented. The results obtained revealed a good temporal and spatial resolution of the flow structure by ECT.

Electrical capacitance tomography (ECT) was used by [24] for imaging various two-phase gas–light oil horizontal flows in a pipe with internal diameter 0.0762 m pressurised test loop. Different flow patterns were established in the test loop by varying the oil and gas flow rates, A comparison of ECT images with those observed through a transparent section and that of prediction of the [25] flow map were presented.

1.2 Predictive models

Mechanistic models give the best predictive capability of flow properties since they depend on the underlying flow physics. One of the most reliable is the two-fluid model where steady state one-dimensional momentum equations are written for each phase and solved simultaneously. For slug flow however, if reliable closures are introduced for slug length, or the length of bubble region, the pressure gradient can be calculated from

the steady momentum balance over a slug unit. Petalas and Aziz [26] utilised such methodology. They calculated the pressure gradient by writing the momentum equation as follows:

$$-\frac{dP}{dz} = \rho_m g \sin\theta + \eta\left(\frac{dP}{dz}\right)_{fr,SL} + (1-\eta)\left(\frac{dP}{dz}\right)_{fr,AM} \quad (1)$$

where the subscript AM refers to the gas bubble assuming it behaves like annular mist flow, and ρ_m is the mixture density and η is an experimentally determined weighting factor that is calculated as follows:

$$\eta = C_L^{(0.75-E_L)} \quad (2)$$

where $C_L = V_{sl}/V_m$ and E_L is the volume fraction calculated using the distribution coefficient C_o, i.e. $E_L = 1 - V_{sg}/C_o V_m$. The restriction for Eq. (2) is that $\eta \leq 1.0$. The frictional pressure gradient for the slug region is calculated using the equation:

$$\left(\frac{dP}{dz}\right)_{fr,SL} = 2\frac{f_{mL}V_m^2\rho_m}{gD} \quad (3)$$

where f_{mL} is the friction factor and it can be reliably calculated using the Blasius relationship which is a sole function of the Reynolds number, i.e.:

$$f_{mL} = 0.046\left(\frac{\rho_m V_m D}{\mu_m}\right)^{-0.2} \quad (4)$$

For the frictional pressure gradient based on annular mist flow, the following relationship is used:

$$\left(\frac{dP}{dz}\right)_{fr,AM} = \frac{4\tau_w}{D} = \frac{2\rho_m f_{mL}V_m^2}{gD} \quad (5)$$

where the subscript f denotes the film region below the gas bubble. Finally, the mixture density and viscosities are obtained from weighted single-phase properties as follows:

$$\begin{aligned}\rho_m &= E_L\rho_L + (1-E_L)\rho_G \\ \mu_m &= E_L\mu_L + (1-E_L)\mu_G\end{aligned} \quad (6)$$

Equations 1–6 have been used by Petalas and Aziz [26] for the pressure gradient and have been used in this work to compare with the experimental measurements. The results are presented in Section 3.

Similarly also used for comparison is the average pressure gradient [27] in a slug unit was obtained by [27] who performed a momentum balance over a global control volume of the slug unit and thus proposed;

$$-\frac{dP}{dx} = 2\frac{f_s}{D}\rho_s U_s^2\frac{\ell_s}{\ell} + \tau\frac{\tau_f S_f - \tau_i S_i}{A_f}\frac{\ell_f}{\ell} \quad (7)$$

where f_s represents the slug friction factor, $\rho_s = \rho_L H_s + \rho_G E_s$ and E_s is the void fraction in the aerated slug. He also noted

that Eq. (7) could also be used to predict the time-average pressure gradient for a fully developed flow in a horizontal pipe.

The slug friction factor f_s is given by the equation

$$f_s = 0.001375\left[1 + \left(2 + 10^4\frac{\varepsilon}{D} + \frac{10^6}{Re_s}\right)^{1/3}\right] \quad (8)$$

2 Experimental setup

2.1 Test facility description

Experiments were conducted in a 0.0762 m–ID horizontal pipe with an L/D ratio of 223. A schematic diagram of the experimental setup is shown in Fig. 3. The measuring section is located at 14 m downstream from the first inlet with a separator, which is used to collect, and the separate the fluid into phases positioned at the end of the pipe.

Mineral oil with brand name CYL680 manufactured by Total Limited UK was used as the liquid phase. It is stored in a tank with a capacity of 2 m³ and fed into the main line through a T-junction by a variable speed Progressive Cavity Pump (MONO CML263) with 17 m³/h maximum capacity. The oil flow rate at the inlet is metered by a Coriolis flow meter (Endress + Hauser, Promass 83F80 DN80), with an accuracy of ±0.35% and recirculated to the oil tank via a by-pass aimed towards achieving a uniform oil viscosity before being injected into the main test line. The oil temperature is regulated using a refrigerated bath circulator (ThermoChill I LR, 230V50Hz PD-1) manufactured by Thermo Fisher Scientific USA.

Compressed air used as the gas was supplied from an AtlasCopco® screw compressor with a maximum supply capacity of 400 m³ /h free air delivery (FAD) and a maximum discharge pressure of 7 barg. The flow rates of this phase was monitored using two flow meters: 0.5-in. vortex flow meter (Endress + Hauser Prowirl 72F15 DN15) and 1.5-in. vortex flow meter (Endress + Hauser Prowirl 72F40 DN40), which ranged from 0 to 20 and 10–130 m³/h respectively.

The two phase flow mixture collected in a separator was allowed to stay for at least 48 h for full phase separation with the gas phase vaporising into the atmosphere leaving behind the liquid phase for reuse.

Pressure gradient was measured using differential pressure transducers (0 ~ 6 bar, PMP1400) installed along the pipe at different locations. The data signals are acquired by via a LabView system connected to a desktop computer while liquid holdup was measured by an Electrical Capacitance Tomography ECT system designed and manufactured by Industrial Tomography System (ITS), UK.
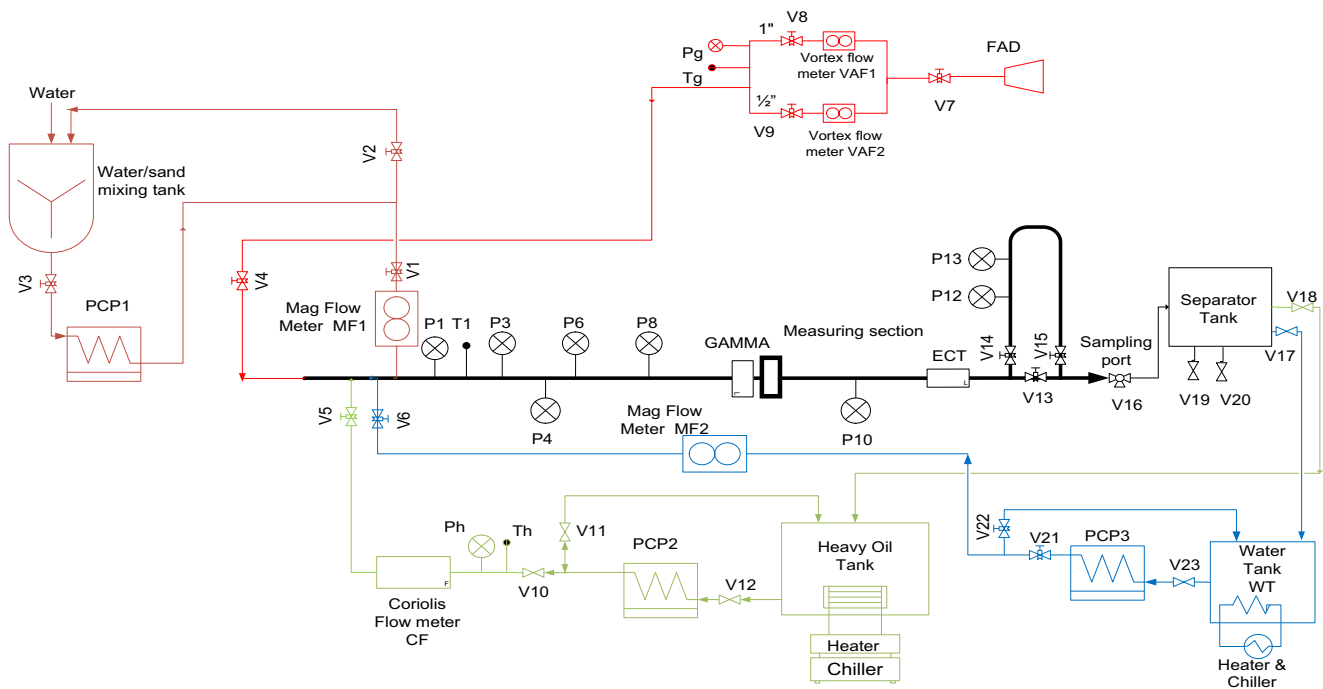
Fig. 3 Schematics of 3-in. experimental facility

2.2 Uncertainty measurements

The Uncertainty of a measured value is an interval around that value such that any repetition of the measurement will produce a new result that lies within this interval. Factors responsible for such differences ranges from changes in temperature, humidity etc. Other factors that may affect measurement results are instrument error, skill of the operator and measurement procedure. Uncertainty of each of the measurement values are shown in Table 1 below; for the direct measurements (pressure gradient, viscosity and liquid holdup), the uncertainty in measurement was obtained from the manufacturers' guide upon a repeatability test conducted to ascertain accuracy of values.

2.3 Experimental procedure

The procedures for an experimental campaign for a particular test matrix starts by visual inspection of the test facility to ensure there are no defects; if any, are duly identified and rectified. The control valves in the flow facility are then open or closed depending on their status order in the rig-operating manual. The computer containing the Labview software is powered on and the software started for flow monitoring and data acquisition. Also, high definition camcorders are setup with adequate lighting at the observation area for video recordings.

The air compressor and oil pump are powered on, the suction valve of the oil pump and the gas flowmeter valves are adjusted to desired flowrates for the test matrix. Data recordings via the LabView software and video recordings are done for all experimental conditions with repetition of the recording procedures until the desired test matrix is completed.

2.4 Test matrix

The test fluid used for this investigation as described in subsection 2.1 above with physical properties at 25 °C given as 917 kg/m^3 and 1.83 Pa.s (Ns/m^2) for density and viscosity respectively. The oil's minimum and maximum viscosity were given as 0.333 and 15.33 Pa.s (Ns/m^2) at temperatures of 50 °C and −2.5 °C respectively. A summary of the test fluid and the matrix used for experimental investigation is presented in Table 2 below.

Table 1 Uncertainty measurements

Measurements	Uncertainty (%)
Superficial liquid velocity	±0.5
Superficial gas velocity	±2.1
Liquid viscosity	± 1.0
Liquid holdup	± 5.0
Pressure drop	± 2.0

Table 2 Experimental test matrix and physical properties of fluid

Test Fluids	Density (kg/m³)	Viscosity (Pa.s)	Test Matrix (m/s)	Interfacial tension (25 °C, N/m)	API Gravity
Air	1.293	0.00017	0.3–10.0	0.033	–
CYL-680	918	1.0 ~ 6.0	0.06–0.3		22.67

2.5 Electrical capacitance tomography (ECT) device

The ECT device used for this investigation was designed and manufactured by Industrial Tomography Systems (ITS), Manchester, UK. The precept of this equipment is based on the permittivity difference of dielectric materials with electrodes lined at the periphery of pipe, for detection of mixture permittivity. With prior calibrations, these signals can be converted to actual concentrations of each phase, and exhibit a distribution through the tomographic technology.

The system is comprised of a sensing unit, data acquisition and a computing system as shown in Figs. 4 and 5. The sensing unit is made up of a flexible copper laminate engraved with a predetermined 12-electrode pattern and placed around the circumference of steel pipe with internal diameter of 0.0762-m. The Computer system has a software; Multi Modal Tomography Console (MMTC) used to view the process of interest online and for tomography data management. Data collated can be assessed offline using Tool-suite V7, another ITS proprietary software.

2.6 Electrical capacitance tomography static calibration test

The calibration of the ECT sensors is done to establish a scale for its tomography display with different phases represented by different code. In this experimental investigation, oil, which has the highest density and permittivity, is coded in red while air with lowest density and permittivity is coded in blue as shown in Fig. 6 below. The test was carried out using the ECT 3-in. sensor, air and mineral oil CYL680 at room temperature. Prior to calibration, the pipe housing with ECT sensors is carefully cleaned and each electrode is connected to the acquisition box in a correct sequence. The low and high reference results are respectively obtained by taking readings from the empty pipe; and when the pipe section is completely filled with oil. Sufficient time is given to ensure that there are no small gas bubbles entrained in the liquid phase.

During an online test, the capacitances between each pair of 12 electrodes are measured, resulting to 66 measurements as an output. Data collected by the ECT acquisition unit is saved to the computer where a cross-section image is reconstructed and displayed using colour codes (i.e. blue for oil and red for gas). By reconstructing image (Linear Back Projection, LBP), the phase distribution over the sensor cross sectional area during measurement is obtained and hence the liquid volume fraction in the pipe can be further estimated. The measured mean liquid holdup estimated from a bench test conducted to mimic stratified and annular flow patterns indicated ±5% uncertainty in measurements as presented in Fig. 7 below. Over 1500 frames of instantaneous liquid holdup are logged to the computer for every experimental flow condition, after which the mean liquid holdup is estimated by averaging the logged data.

3 Experimental results and discussions

The test results for this experimental investigation of viscous oil-gas two-phase flow are presented in this section. It is
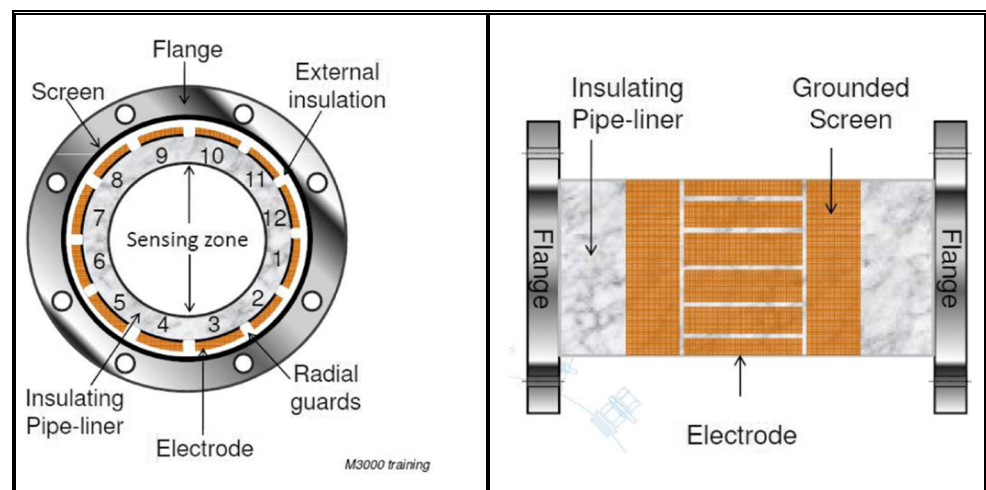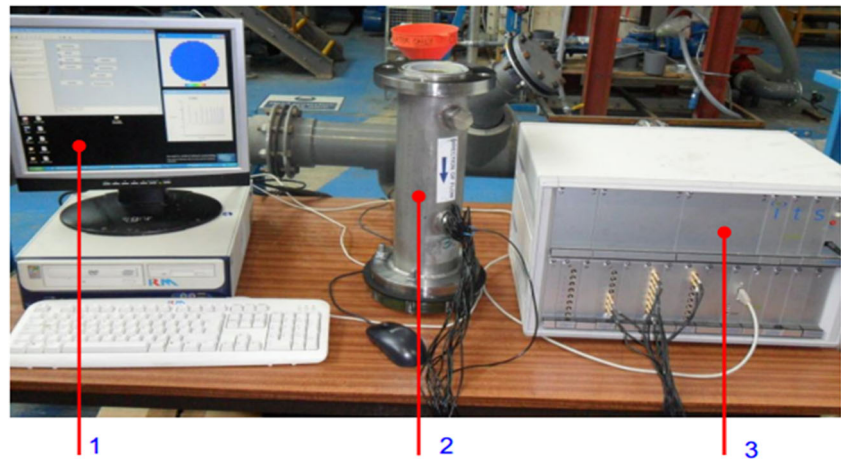

Fig. 4 An archetypal ECT system and sensor arrangement

Fig. 5 ECT System; (1)-Computer System, (2)-ECT Sensors embedded in pipe and (3)-Data Acquisition System

outlined into flow patterns, pressure gradient, mean liquid holdup and slug frequency and slug liquid holdup. The results obtained are subsequently compared with predictions from existing models and correlations in the literature to access their performance for high viscosity oil data.

3.1 Flow pattern visualization

For flow visualization, a High definition, 60GB HDD Sony camcorder, DSCH9 with 16 megapixels was used for video recordings during the test to aid visual observations for the flow patterns. Plug flow, slug flow, pseudo slug and wavy annular flow patterns were observed for this investigation. Both plug flow and slug flow in this paper, are termed as "intermittent flow". To start with, intermittent flow tends to dominate the entire flow regime. It is a flow pattern characterised by an intermittent passage of an elongated liquid body containing some dispersed bubbles alternating with sections of separated flow (i.e. film region). The film region is characterised by the stratification of oil and gas owing to gravity effects such that the less dense phase (i.e. gas) flows at the top while the denser phase (i.e. oil) flows at the bottom of the pipe. This is closely followed by a flow pattern termed as "pseudo slug". It is a transition flow pattern from the intermittent flow pattern to wavy-annular flow pattern and it is observed with a continuous increase in the gas superficial velocity. It is generally characterised by large energetic travelling waves. Again, further increasing the superficial gas velocity results in the oil phase been lifted by the highly turbulent gas phase which brings about the formation wavy-annular flow
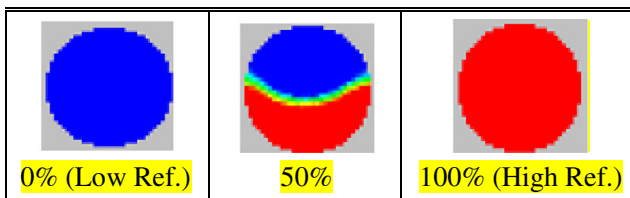
characterised by a rolling wave at the interface. Figure 8 shows snapshots of the flow patterns observed for this investigation.

3.2 Flow characterization by ECT

Electrical Capacitance Tomography (ECT) instrumentation earlier described in subsection 2.5 above was also used for flow pattern identification and validation of visual inspection. Over 1000 raw capacitance data from the ECT were obtained for each flow condition and consequently analysed. Stacked tomographic images and tomograms as presented in Fig. 8 represent the observations for the experimental investigation.

The reconstructed images illustrate the instantaneous time-varying phase distribution in the pipe and consequently, the flow patterns. From the calibration as described in sub-section 2.6, a completely red colouration of the tomogram indicates 100% oil while a completely blue colouration tomogram indicates 100% gas. Four characteristic flow patterns described below were captured by the tomograms:
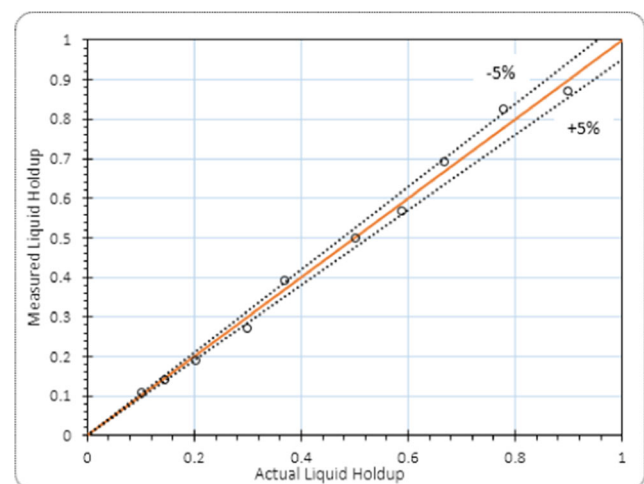

Fig. 6 ECT Tomographic Image Display

Fig. 7 Calibration of the ECT system

Fig. 8 Flow Pattern illustration from ECT Stacked Images/ tomograms and video recordings

Fig. 8 Flow Pattern illustration from ECT Stacked Images/ tomograms and video recordings

Plug Flow: This flow pattern is characterized by two distinct tomographic images that are displayed intermittently. A tomogram showing a segregated layer of red at the bottom (i.e. Suggestive of oil) with blue coloration

(i.e. indicative of gas) at the top section of the pipe. At intervals, the image changes to almost completely to red (oil), indicating the passage of an elongated liquid body with insignificant amount of gas through the ECT pipe
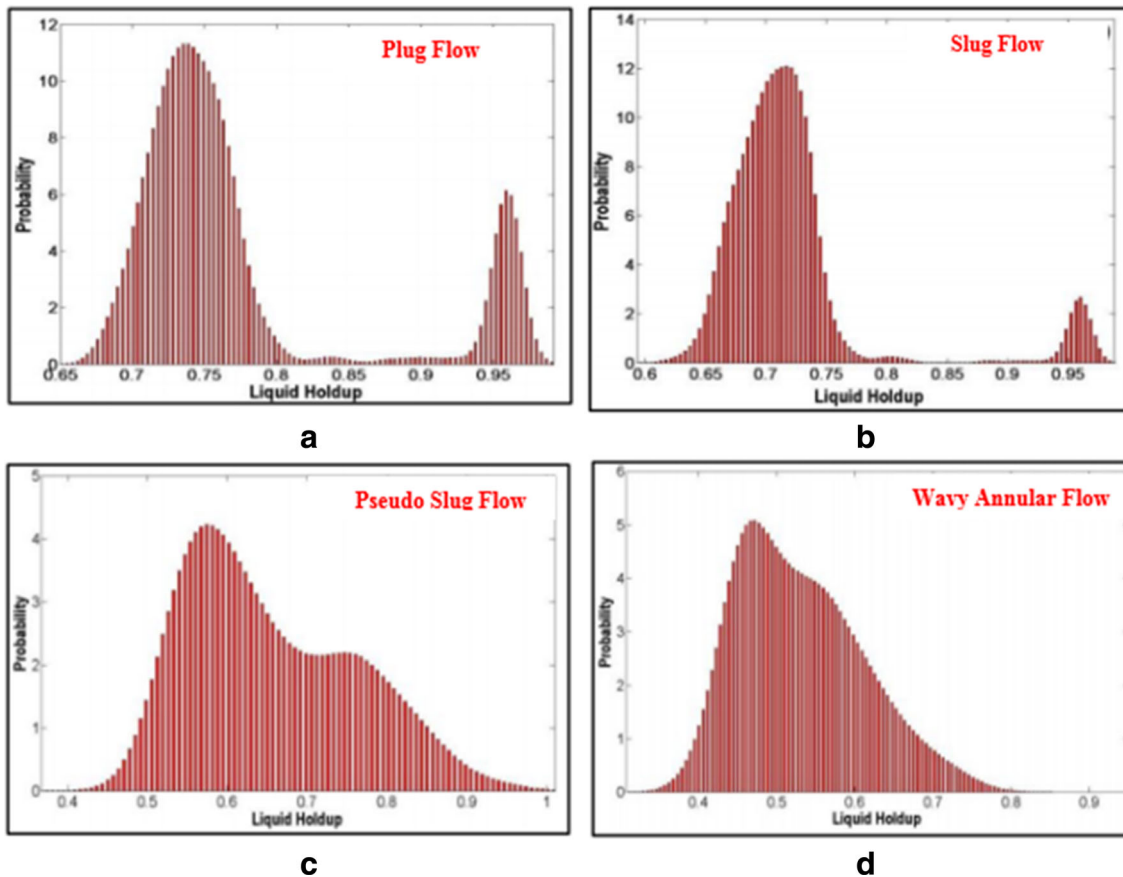
Fig. 9 Probability Density Function (PDF) obtained ECT liquid holdup

walls. For the stacked images, as presented in the figure above, oil (red colour) was observed to completely bridged the pipe with passage of the elongated liquid body through the device. This flow pattern was classified as plug flow based on the description provided by [28]

Slug Flow: The distinguishing parameter for this flow pattern, which is similar to plug flow, is the presence of pronounced gas entrainments as indicated by the small blue coloration in a largely red tomogram. A further observation of the stacked tomograms for this flow pattern indicates clearly the gas entrainments during the passage of t slug.

Pseudo-Slug Flow: On further increase in the superficial gas velocity, the pseudo –slug flow pattern is observed. The red section (oil) of the tomogram is seen to have insufficient energy to bridge the blue section (gas core). The amplitude of the waves at the interphase are not high enough to bridge the top of the pipe on most occasions, though succeeding a few times but with small red section

bridging the pipe. An observation noted on an infrequent basis.

Wavy Annular Flow: Again, further increase in the gas phase results in the formation of wavy annular. Here as can be seen from Fig. 8, the gas momentum is high enough to sweep the liquid to the top of the pipe. A yellowish-green colour was observed at the top of the pipe while red (oil) flowed most at the bottom.

Further statistical analysis of the ECT liquid holdup plots was carried out in order to distinguish the various observed flow patterns using the Probability Density Function (PDF) as shown in Fig. 9. PDF has been broadly used by different researchers [29, 30] for the identification of two-phase gas-liquid flow patterns. It is a function that gives the probability for each value of a random variable, expressed as $f(x)$ of a discrete random variable (X) given by $f(x) = P(X = x)$ for all x, where x in this case is the ECT liquid holdup. For intermittent flow (i.e.

Fig. 10 Flow pattern maps for gas-liquid two-phase flow (**a**) @3.0–3.5 Pa.s (**b**) @5.1–5.5 Pa.s
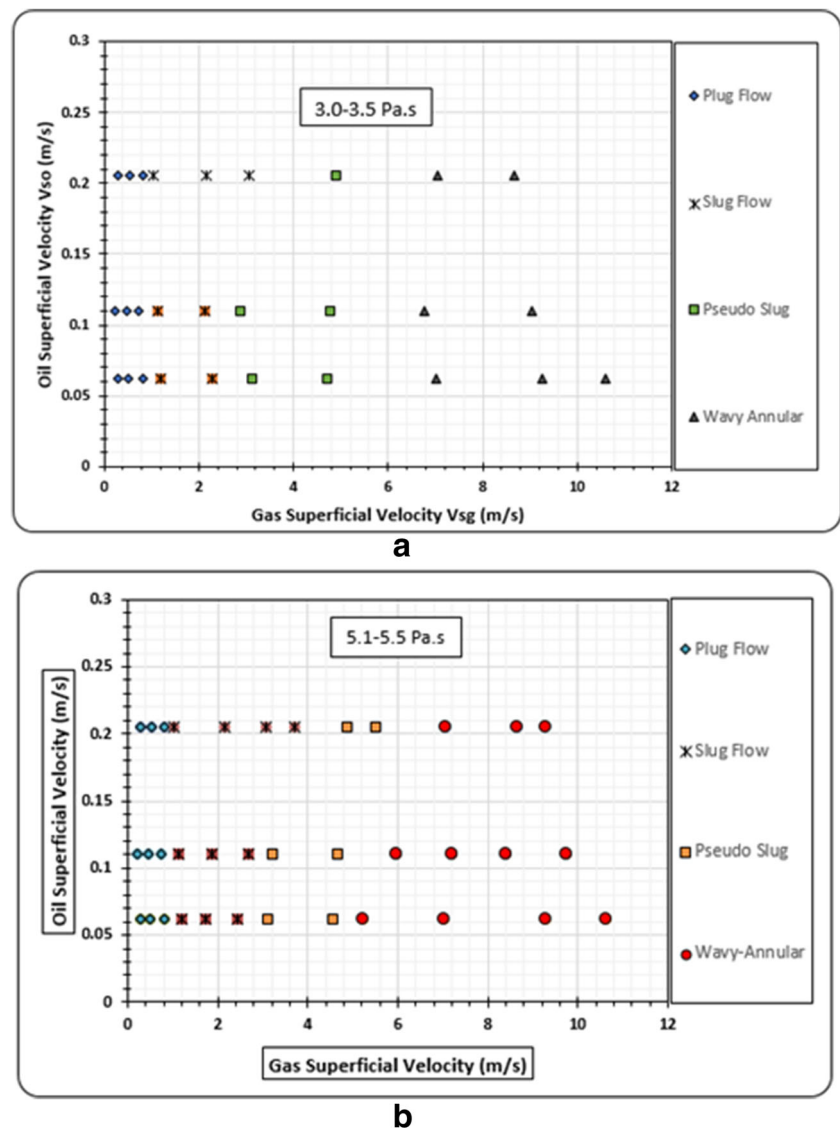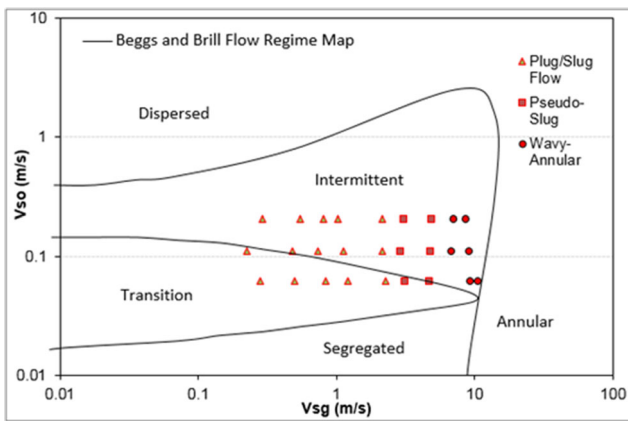
Fig. 11 A Comparison of experimental data points superimposed on the Beggs & Brill, [32] flow pattern map

Slug/plug flows as shown in Fig. 9), the PDF has a bi-modal distribution. The two-peak structure is a qualitative confirmation of visually observed intermittent flow pattern (plug and slow pattern). The closest peak to the ECT liquid holdup values of 1 is indicative of the elongated liquid body while the liquid film section of the slug unit is represented by the other peak. Slug flow was distinguished from plug flow its dominance of the film region for the former in addition to a relatively smaller elongated liquid body due to increased gas entrainment. Figure 9 (C) represents a pseudo-slug flow pattern and it exhibits transition flow characteristics by combining the features of slug and annular flow. A gradual flattening out of the smaller peak at high liquid holdup values occurs. The unimodal distribution as illustrated by (D) is indicative of annular flow.

Figure 10 shows the flow pattern maps constructed for the observed flow regimes using abscissa for the superficial gas velocities and ordinate for the superficial oil velocities. From
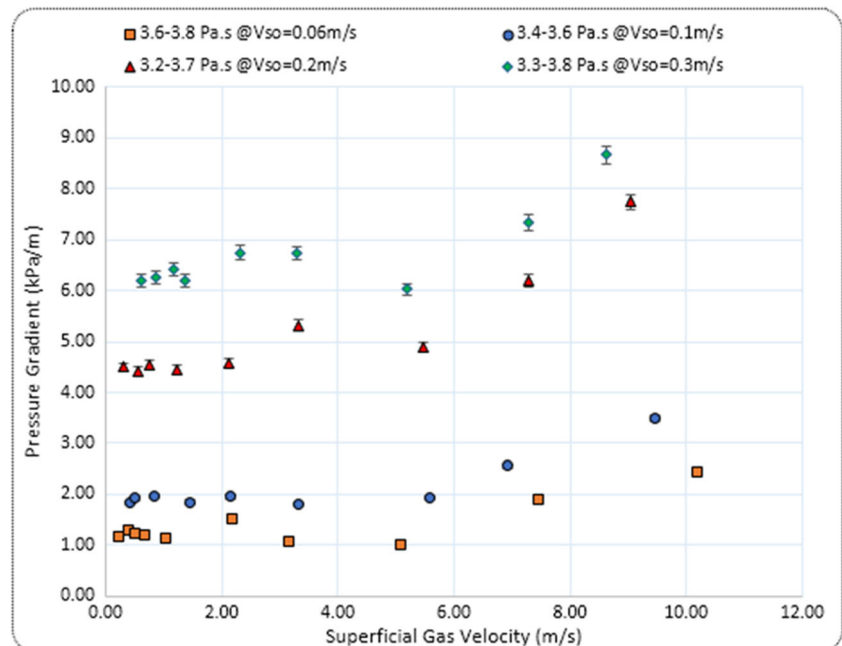
the figure, it is observed that an increase in the superficial oil velocity increases the tendencies and existence of intermittent flow region since slug formation is the function of liquid height. Correspondingly, as the viscosity of liquid is increased, the intermittent flow region is enhanced. This can be attributed to the fact that an increase in liquid viscosity results in increased shear on the pipe walls the pipe thus; the in-situ liquid velocity is decreased in the process. Similar findings have been reported by [6, 8, 21, 31].

In Fig. 11, a comparison of observed flow pattern against the prediction by flow regime map proposed by [32] is presented. As can be seen, the flow pattern map by [32] shows some discrepancies in the prediction of the flow regimes for this experimental investigation. The transition from intermittent to annular flow is over predicted by the map and this could be attributed to viscosity and diameter effects.

3.3 Pressure gradient

Measured pressure gradient plotted as function of superficial gas velocity (Vsg) for varying superficial oil velocities (Vso) is presented in Fig. 12. From the figure, it is evident that the measured pressure gradient has strong dependency on the flow pattern. The trend exhibits a slight increase in pressure gradient as superficial gas velocity increases in the intermittent flow pattern region. Beyond this point, the said increase in measured pressure gradient is observed to steepen as the gas superficial velocity increases corresponding to the region of wavy-annular flow pattern region. This can be credited to the fact that most of the oil flow around the walls of the pipe thereby increasing resistance to flow owing to increased shear around the pipe walls.

Fig. 12 Pressure gradient as a function of gas superficial velocity for different oil superficial velocity @ 3.4–3.8 Pa.s

Fig. 13 Pressure gradient as a function of gas superficial velocity for different oil superficial velocity @ 4.2–4.6 Pa.s
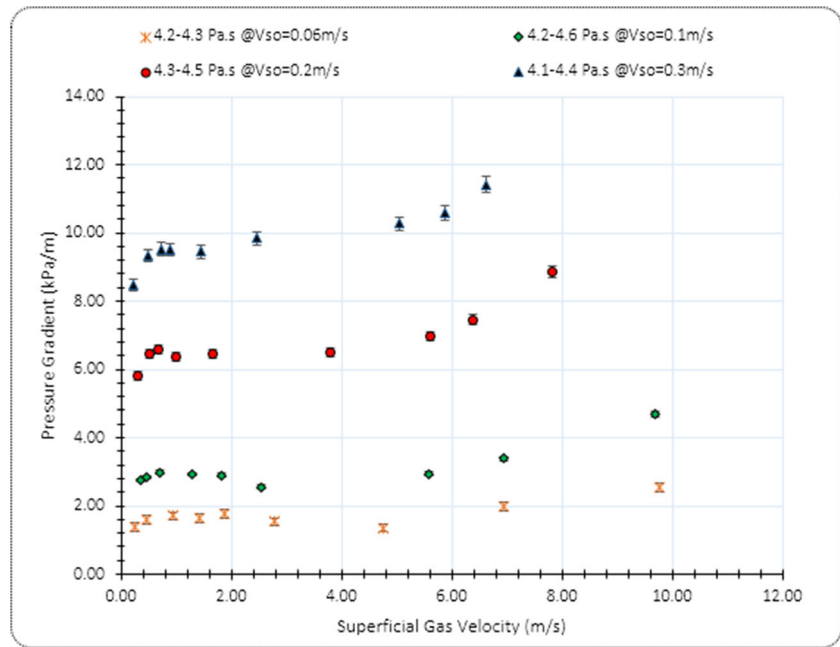
Similarly, from Figs. 12 and 13, the measured pressure gradient also increases with an increase in oil superficial velocity and oil viscosity. Increase in oil viscosity or oil holdup enhances the resistance to flow which results in higher pressure gradients. The observed trend for this investigation is consistent with those reported by [7, 14, 15, 31, 33].

Figure 14 below shows a comparisons between present experimental data for pressure gradient and those of [8, 34, 35]. Pressure gradient is seen to increase with increase in liquid viscosity; this is associated with the increased viscous shear around the pipe walls. On the other hand, pressure gradient increases with an increase in the superficial gas velocity

at a fixed liquid superficial velocity and this is expected considering the fact the pressure gradient is directly proportional to the square of flow velocity. It is however observed that the pressure gradients increasing trends at much higher viscosity are not always smooth as there are fluctuations reflecting the complexity and chaotic nature of the dominant flow pattern associated with high liquid viscosity as earlier explained.

Figures 15 and 16 show a comparison between measured pressure gradient and prediction by the theoretical models developed by [26, 27] plotted as a function of mixture velocity. For both models as demonstrated by the figures, there is a huge disparity between experimental measurements and those

Fig. 14 Comparison of measured pressure gradient and previous pressure gradient plotted as a function of superficial gas velocity
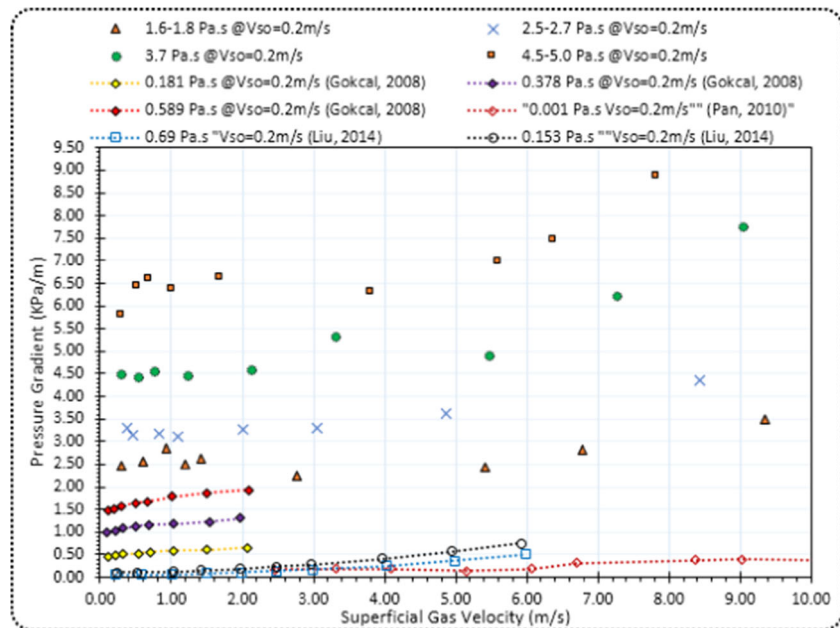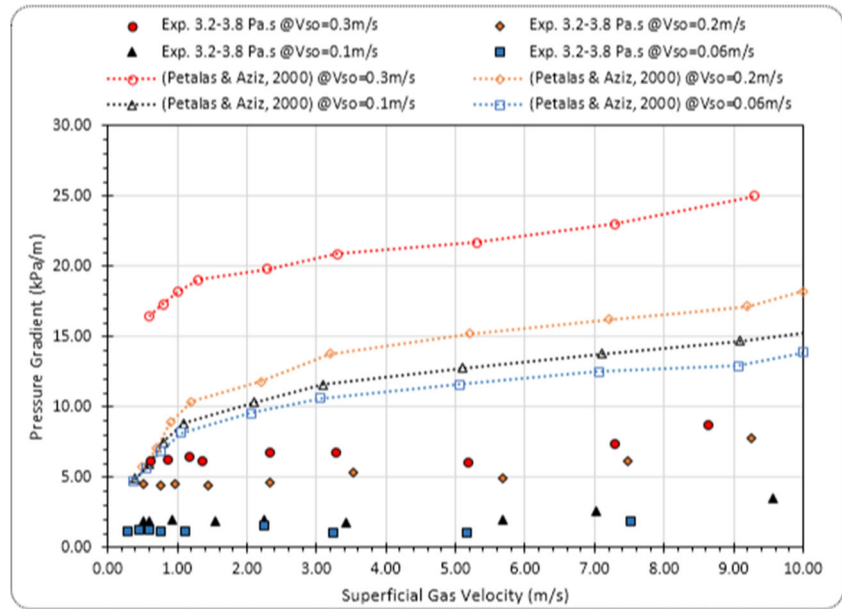
Fig. 15 Comparison of measured pressure gradient with the prediction by [26]

of the prediction models. It is also observed that the disparity steepens most especially for [26] at high mixture velocity thus indicative of the fact that, for high viscosity liquids data, these theoretical models are not valid as such will require improvement for accurate prediction of pressure gradient in unconventional oil resources.
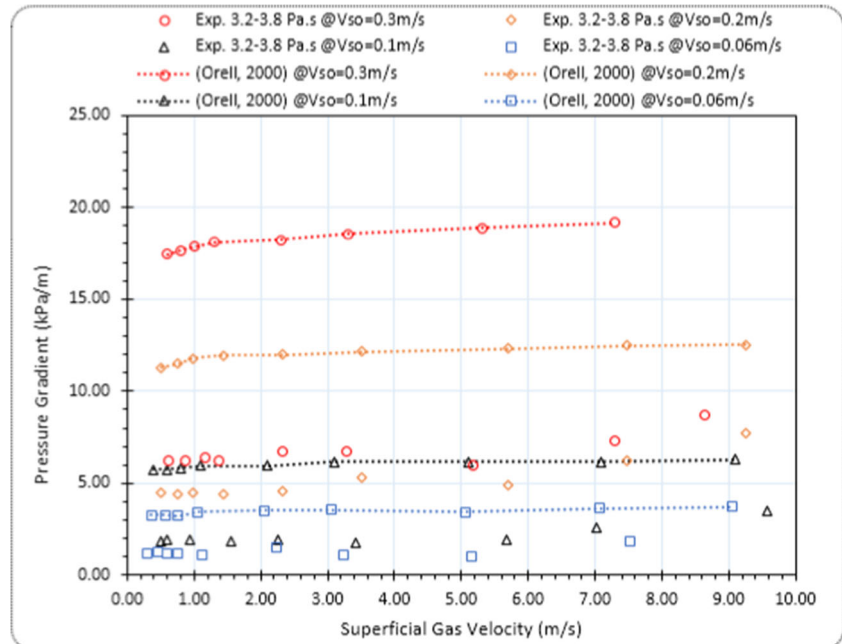
3.4 Mean liquid holdup

This important two-phase flow parameter was obtained by taking the average of the time varying instantaneous liquid holdup measured by ECT. If the instantaneous volumetric fraction of the liquid phase in the cross sectional are of the

ECT is represented by h_a, then the average phase volumetric fraction of the liquid (i.e. mean liquid holdup) over a period of time series recorded (T) can be calculated for each experimental flow condition. Assuming the total number of data points recorded for a test period is (N). Then the mean liquid holdup over the whole time period H_a can be estimated using:

$$H_a = \frac{1}{T} \int_T h_a dt = \frac{1}{N} \sum_{n=1}^{N} h_a \qquad (9)$$

Figure 17a shows a general trend of reduction of measured mean liquid holdup as the superficial velocity of gas increases. The decrease can be attributed to the gas phase occupying more

Fig. 16 Comparison of measured pressure gradient with the prediction by [27]

volume fraction in the cross-sectional area of the pipe thus reducing the liquid content. As expected, an increase in the superficial liquid velocity results to an increase in the mean liquid holdup owing to increased liquid height. The trend observed for the measured mean liquid hold up is in agreement with the findings of [8, 10, 13, 34, 35]. The error bars represent the maximum uncertainty in holdup measurement by the ECT sensors. This was validated by a triplicate of measurements for each condition, which were within 5% of each other. Similarly, as the oil viscosity increases as shown in Fig. 17b there is a corresponding slight increase in the measured mean liquid holdup at fixed superficial liquid velocity. This is credited to increased viscous drag on the pipe walls, which results in decreasing the liquid velocity thereby increasing the liquid holdup.

It is however observed from both plots that, the mean liquid holdup in the intermittent flow region exhibits slight dependency on viscosity and velocity of liquid. In the intermittent flow region, the effects of viscosity is subtle as against the pronounced tendency in the wavy-annular region. This is an indication that increasing gas velocity only causes a little effect on mean liquid holdup for slug and annular flow. The possible reason for this could be credited to the fact the process of liquid deposition dominates in the wavy-annular flow region, which is driven by the high momentum of the gas energy, rather than viscous forces energy induced by the liquid film. Though the mean liquid holdup decreases with a relatively steep slope in the intermittent flow region, it still travels and deposits around the pipe wall due to its adhesive property,

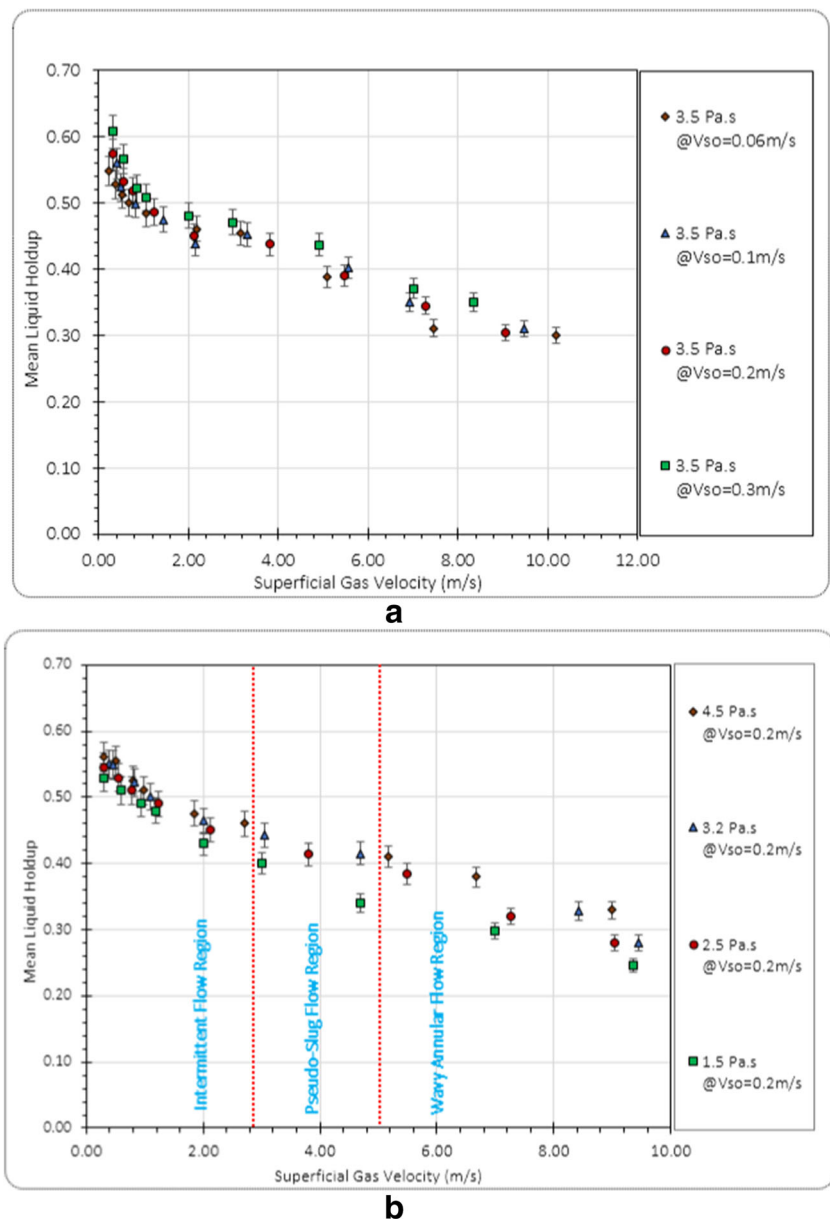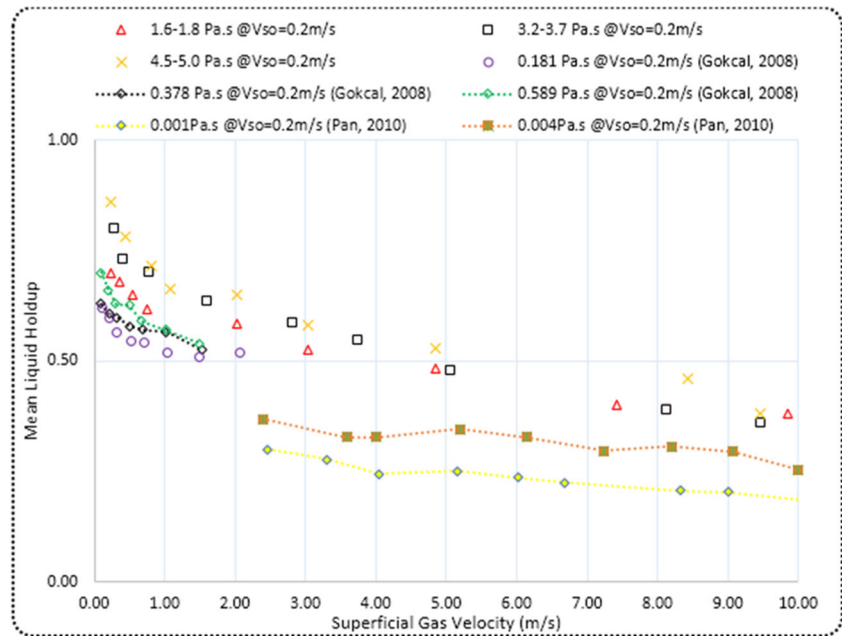Fig. 17 Mean liquid holdup plotted as function of superficial gas velocity

Fig. 18 Comparison of mean liquid holdup with those in the literature


resulting to small reduction in the whole superficial gas velocity range for intermittent flow region.

Figure 18 shows a comparison of the measured mean liquid holdup with those of [8, 34] plotted as a function of gas superficial velocity. As can be seen from the plot which exhibit similar trend of reduction as those compared with. Again, liquid viscosity is seen to play a significant role of increasing the mean liquid holdup as viscosity increases. This is ascribed to increase in viscous drag around the pipe walls and hence resistance to flow.

The few correlations for the prediction of liquid holdup that exist in the literature were tested with the present experimental

data. Two categories of these models were identified. In the first category, two fluid models for which the models of [17, 32] were considered while the drift flux prediction models of [36–38] were considered in the second category. While the choice of [32] prediction model is based on the fact that it is widely used and acceptable for the calculation of liquid holdup in the petroleum industry, [37] was chosen because a relative higher viscosity liquid was used for the study. Results of comparison shown in Fig. 19 indicates that all the models tested predicted the present data with different degrees of discrepancies. This can be attributed to the fact that there were all developed based on observation of low viscous liquids. The

Fig. 19 Comparison of measured mean liquid holdup with those of prediction models
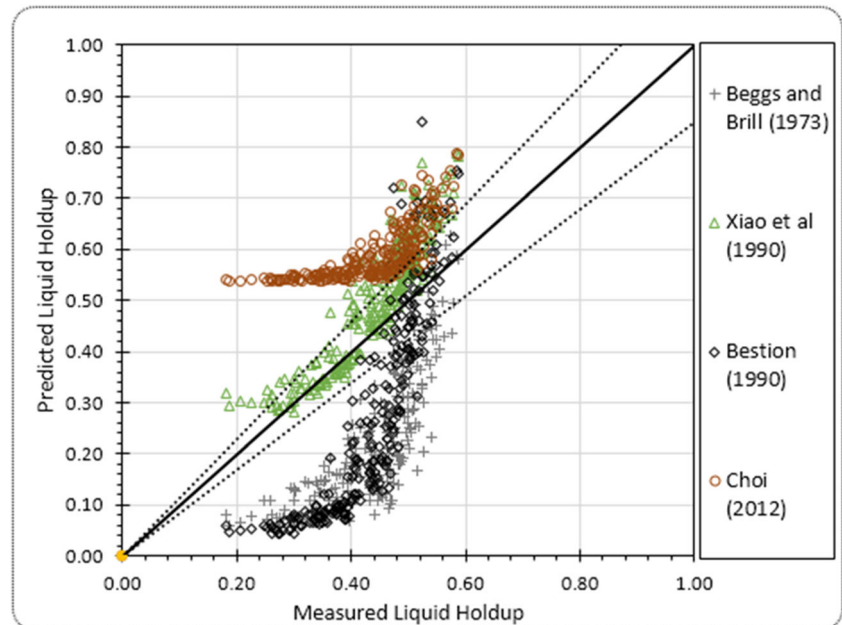
model by [17] performed better when compared to others, probably because it accounted for some characteristic features of slug flow bearing in mind that slug flow is the dominant flow pattern for high viscosity oil.

3.5 Slug frequency

A typical plot from of the ECT instantaneous liquid holdup time series plot exhibits an intermittency behavior for slug flow. This is characterized by passage of crests and troughs. The crests region is indicative of the passage of slug liquid body usually have higher liquid holdup value as compared with the troughs region which suggests the slug film region

and have relatively lower liquid holdup. slug frequency is obtained by counting the quantity of instantaneous slug liquid body passing over a period of time, this is validated by counting the number of slugs body from the recordings using high definition video camera recordings. To differentiate travelling waves from slug liquid body most researchers are known to have adopted specific values representing a threshold for slug count. For this study, the technique used by [7, 39] was adopted. This technique defines the threshold for liquid holdup in the slug body and slug film region P_{th} by the expression. Where P_{th} is the instantaneous liquid holdup measured using the ECT and P_a is the time series ECT measurement.

Fig. 20 **a** and **b** Slug frequency as a function of gas superficial velocity
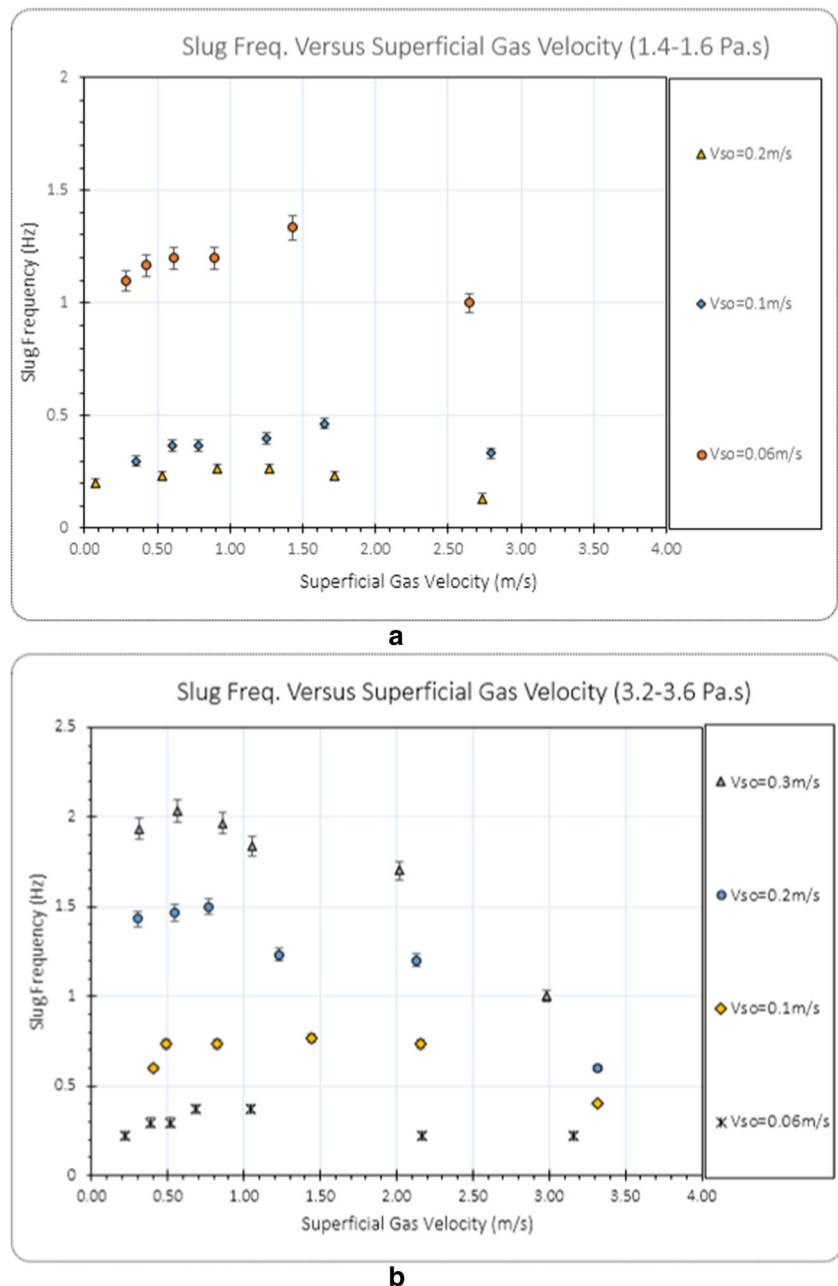
$$P_{th} = \frac{1}{2} [max(P_a) + min(P_a)] \qquad (10)$$

From Fig. 20a and b below showing a plot of slug frequency as a function gas superficial velocity indicates a general initial increase in slug frequency followed by a decreases as gas superficial velocity increases. This can be ascribed to the fact that the liquid content in the pipe reduces as more gas phase occupies the cross-section of the pipe thereby sweeping out most of the liquid content, which is a primary function of slug formation. Similarly, increase the liquid content results in increase in slug frequency within same flow condition; this is because of increase in the input of the liquid content, which then translates into higher liquid film height in the pipe.

Similarly, it is obvious from both plots that slug frequency increases when liquid viscosity is increases. This can be explained by the fact that the liquid level in the pipe cross section increases when viscosity increases owing to resistance to flow. When this happens the probability for slug formation is enhanced and hence slug frequency. The reported findings are in agreement with those of [13, 14, 40].

Presented on Fig. 21 above is a plot comparing the measured slug frequency for this study and those of [8, 34] for different liquid viscosities. The plot exhibits a similar increasing pattern as viscosity increases and a decrease in the measured slug frequency with increasing superficial gas velocity credited an increase in more of the gas phase occupying the cross sectional area of the pipe thus sweeping out more of the liquid phase. A detailed comparison and performance evaluation of existing slug frequency prediction models against measured slug frequency have been conducted by [4]. The error bars show the uncertainty in determining the slug frequency using the ECT system. To estimate this error, we compared the ECT slug frequency and manual counting of slug units using video camera recording of the flow. In each case, 60 slug units were counted and a maximum difference of 3 slug units were observed giving a maximum value of 5% error in slug frequency.

3.6 Slug liquid holdup

This is the liquid holdup in the slug body. Figure 22a shows the mean slug holdup measured by ECT plotted as a function of the gas superficial velocity. Within the experimental test matrix as can be seen from the plot, slug liquid holdup generally decreases with increase in superficial gas velocity, as earlier explained, this is as a result of sweeping of most of the liquid phase from the pipe resulting to more of the gas phase occupying the pipe cross sectional area. However, an increase in viscosity results in a slight increase in slug liquid holdup. This can be credited to the increase in shear around the pipe wall as viscosity increases thereby limiting free flow. In addition, it is observed in Fig. 22b that there is a slight increase in the slug holdup as the superficial oil velocity is increased. This is expected as an increase in superficial liquid velocity generally result in an increase in the input of liquid content in the pipe.

A comparison between the measured slug liquid holdup for this this study and those of [34, 41] is presented in Fig. 22c. The plot exhibits a general trend in reduction of the mean slug liquid holdup with a corresponding increase in the gas superficial velocity. However, it is observed that as liquid viscosity increases, there is a just a slight increase in the mean liquid slug holdup when compared with low viscous liquid as in the case of the data points from [34].

Fig. 21 Comparison of measured Slug frequency with those in the literature
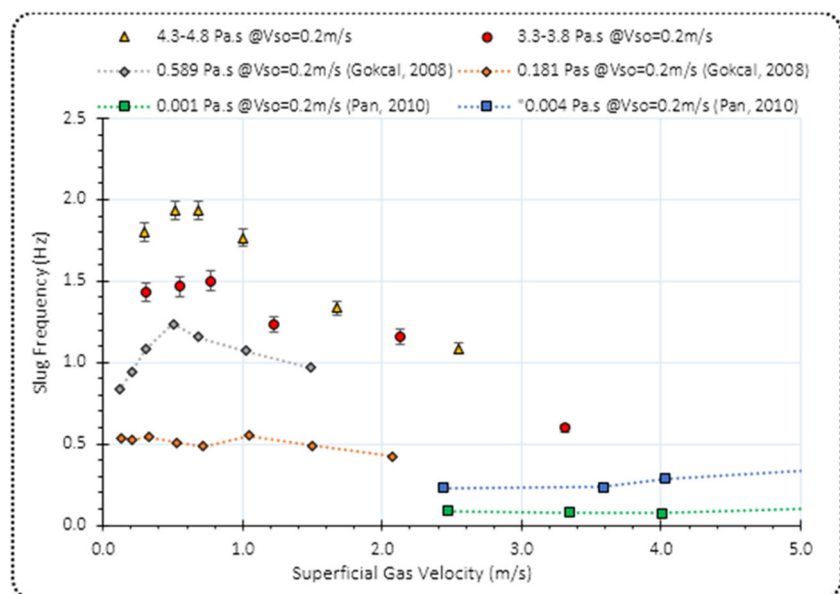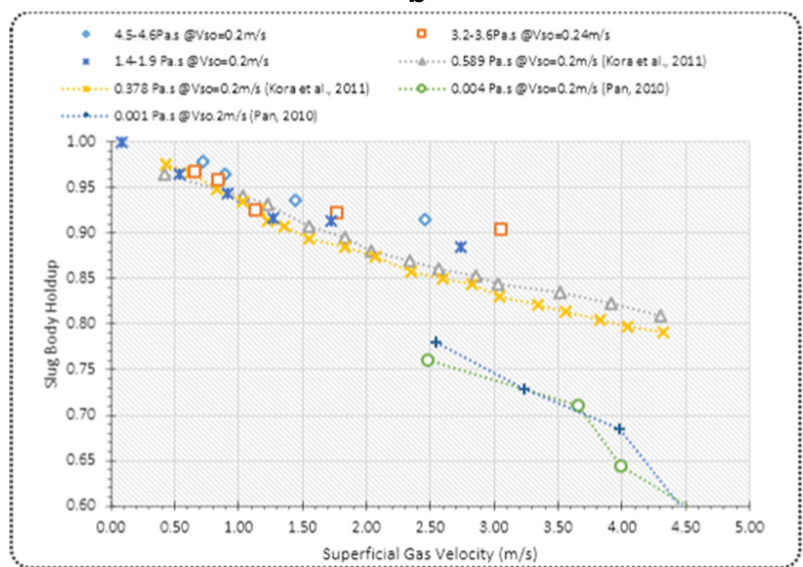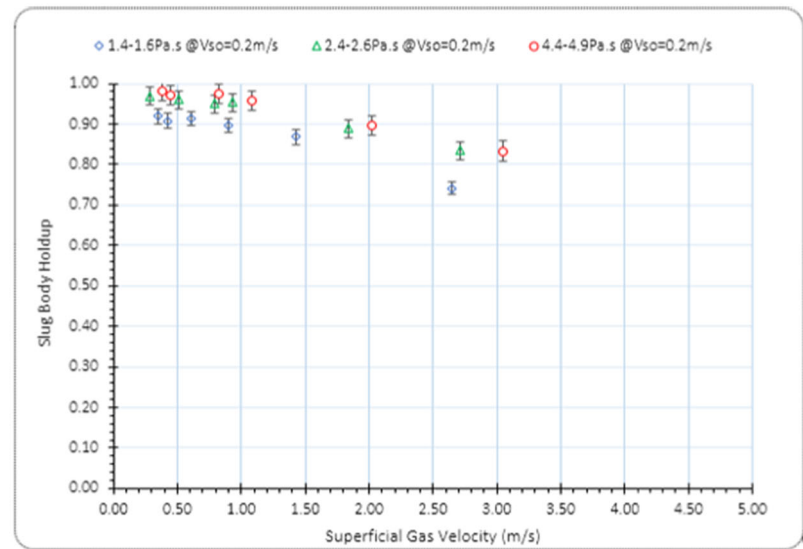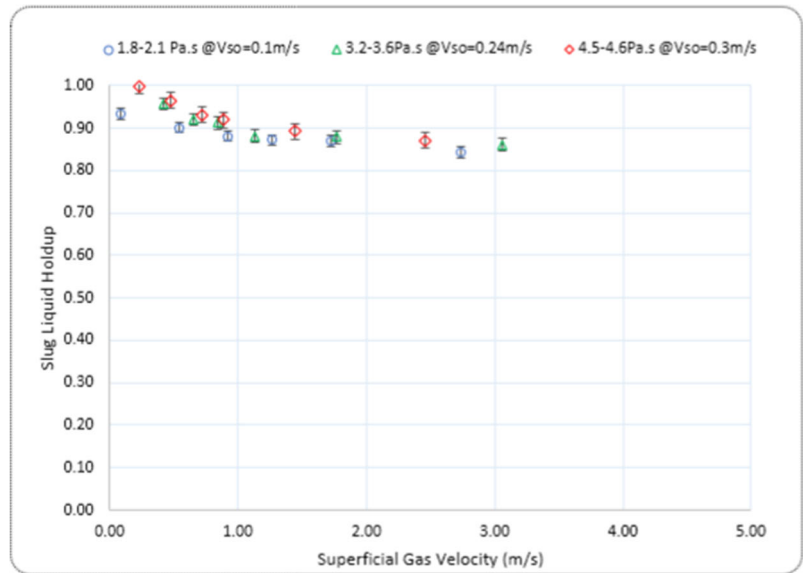
Fig. 22 Slug liquid holdup and slug body holdup plotted as a function of gas superficial velocity

a

b

c
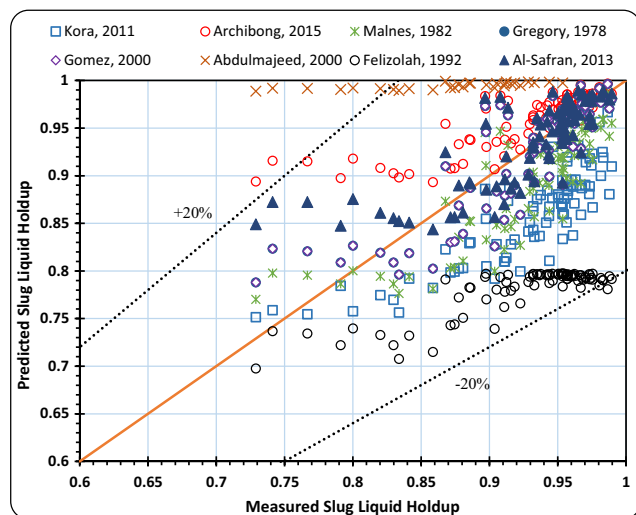
Fig. 23 Measured slug liquid holdup versus prediction models

characteristics) on liquid viscosity effects. A comparison of the experimental liquid holdup with existing correlations showed the inadequacy of their application for high viscous oil flow with the correlation of [17] been the best performing within an error margin of ±15%. However, for the slug liquid holdup, existing correlations showed good agreement with the present experimental results as most were predicted to within ±20%. Finally, existing slug frequency prediction methods gave consistent under predictions of the high viscosity values obtained for this study and these correlations should be used with caution in such cases and should be updated in future studies.

Compliance with ethical standards

Conflict of interest None declared.

A comparison was carried out between the measured slug holdup and existing prediction models in the literature. The performance of the following models [6, 41–46] were assessed as illustrated in Fig. 23. It is worth noting that other than the prediction models of ref. [6, 41, 43] the rest were developed from and validated against low viscosity liquid data. Results shows that all the models tested over-predicted and in some cases under prediction of the present slug holdup data with different magnitude. Al-Safran et al. [43] had the best performance with some over predictions attributable to the viscosity difference in the oil used while [46] showed the farthest prediction.

4 Conclusion

Experimental investigations to study the effects of liquid viscosity on two-phase oil-gas flows have been carried out using Electrical Capacitance Tomography (ECT) for which flow patterns identified and validated through visual observations and video recordings included intermittent, pseudo-slug and wavy annular flows. Mean liquid hold up and slug liquid holdup were also measured by means of ECT. The obtained results illustrate a general trend of reduction in the measured mean liquid holdup value with increase in the gas superficial velocity and that viscosity has little effect on holdup. Slug frequency estimated from ECT measurement and validated by slug counts from video recording exhibited a general increasing trend with liquid input and viscosity. Measurements of pressure gradient were done by means of differential pressure transducers. The results obtained showed that pressure gradient increases with an increase in superficial liquid velocity. Comparison between experimental measurements for this study has further highlighted the significant dependency of all the measured parameters (most significantly slug flow

References

1. Alboudwarej H, Felix J, Taylor S, Badry R, Bremner C, Brough B, Beshry M (2006) Highlighting heavy oil. Oilfield review 18(2):34–53
2. Richard M, Emil A (2003) Heavy oil and natural Bitumen-strategic petroleum resources, *U.S. Geological Survey Fact Sheet 70–03, Eastern Publications Group*, [Online]. Available: http://pubs.usgs.gov/fs/fs070-03/fs070-03.html. [Accessed 27 Jun 2013]
3. Meyer RF, Attanasi, ED, Freeman PA (2007) Heavy oil and natural bitumen resources in geological basins of the world: U.S. Geological Survey Open-File Report 2007-1084, available online at http://pubs.usgs.gov/of/2007/1084/
4. Baba YD, Archibong AE, Aliyu AM, Ameen AI (2017) Slug frequency in high viscosity oil-gas two-phase flow : experiment and prediction. Flow Meas Instrum 54(2016):109–123
5. Baba YD (2016) Experimental investigation of high viscous multiphase flow in horizontal pipelines. PhD Thesis, Cranfield University
6. Archibong A (2015) Viscous multiphase flow characteristics in pipelines. PhD Thesis, Cranfield University, United Kingdom
7. Zhao Y (2014) High viscosity liquid two-phase flow. PhD Thesis, Cranfield University, United Kingdom
8. Gokcal B (2008) An experimental and theoretical investigation of slug flow for high oil viscosity in horizontal pipes. PhD Thesis, The University Tulsa, USA
9. Weisman J, Duncan D, Gibson J, Crawford T (1979) Effects of fluid properties and pipe diameter on two-phase flow patterns in horizontal line. Int J Multiphase Flow 5(C):437–462
10. Nadler M, Mewes D (1995) Effects of the liquid viscosity on the phase distributions in horizontal gas-liquid slug flow. Int J Multiphase Flow 21(2):253–266
11. Crowley CJ, Sam RG, Walliis GB, Metha DC (1985) Slug flow in large diameter pipe. American Institute of Chemical Engineers Conference, No. CONF-841121, New York, NY
12. Sam RG, Crowley CJ (1986) Investigation of two-phase flow processes in coal slurry/hydrogen heaters. Hanover, NH

13. Brito R, Pereyra E, Sarica C (2013) Effect of medium oil viscosity on two-phase oil-gas flow behavior in horizontal pipes. In Offshore Technology Conference, p. 285

14. Gokcal B, Wang Q, Zhang H, Sarica C (2006) Effects of high oil viscosity on oil / gas flow behavior in horizontal pipes. In SPE Annual Technical Conference and Exhibition

15. Foletti C, Farisè S, Grassi B, Strazza D, Lancini M, Poesio P (2011) Experimental investigation on two-phase air/high-viscosity-oil flow in a horizontal pipe. Chem Eng Sci 66(23):5968–5975

16. Farsetti S, Farisè S, Poesio P (2014) Experimental investigation of high viscosity oil–air intermittent flow. Exp Thermal Fluid Sci 57: 285–292

17. Xiao JJ, Shonham O, Brill JP (1990) A comprehensive mechanistic model for two-phase flow in pipelines. In SPE Annual Technical Conference and Exhibition

18. Zhang H-Q, Wang Q, Sarica C, Brill JP (2003) Unified model for gas-liquid pipe flow via slug dynamics—part 1: model development. J Energy Resour Technol 125(4):266–273

19. Losi G, Arnone D, Correra S, Poesio P (2016) Modelling and statistical analysis of high viscosity oil / air slug fl ow characteristics in a small diameter horizontal pipe. Chem Eng Sci 148:190–202

20. Archibong A, Zhao Y, Yeung H (2014) Comparison of electrical capacitance tomography & gamma densitometer measurement in viscous oil-gas flows. AIP Conf Proc 1592(1)

21. Zhao Y, Lao L, Yeung H (2015) Investigation and prediction of slug flow characteristics in highly viscous liquid and gas flows in horizontal pipes. Chem Eng Res Des 102:124–137

22. Areeba S, Ismail I, Mohd NK (2010) Study of void fraction measurement in a two phase flow by using differential pressure and electrical capacitance tomography. In Fourth Asia International Conference on Mathematical/Analytical Modelling and Computer Simulation (AMS)

23. Hunt A, Pendleton J, Ladam Y (2004) Visualization of two-phase gas-liquid pipe flows using electrical capacitance tomography. In Proceeding of ESDA2004 7th Biennial ASME Conference on Engineering Systems Design and Analysis. pp 1–5

24. Gamio J, Castro J, Rivera L, Alamilla J, Garcia-Nocetti F, Aguilar L (2005) Visualization of gas-oil two-phase flows in pressurized pipes using electrical capacitance tomography. Flow Meas Instrum 16: 129–131

25. Taitel Y, Dukler AE (1976) A model for predicting flow regime transitions in horizontal and nearhorizontal gas-liquid flow. AICHE J 22(1):47–55

26. Petalas N, Aziz K (2000) A mechanistic model for multiphase flow in pipes. J Can Pet Technol 39(6):43–55

27. Orell A (2005) Experimental validation of a simple model for gas – liquid slug flow in horizontal pipes. Chem Eng Sci 60:1371–1381

28. Barnea D (1987) A unified model for predicting flow-pattern transitions for the whole range of pipe inclinations. Int J Multiphase Flow 13(1):1–12

29. Hernandez PV (2007) Gas-liquid two-phase flow in inclined pipes. PhD Thesis, University of Nottingham

30. Arubi T, Yeung H (2011) Gamma radiation methods in characterizing horizontal and vertical multiphase flow. In Offshore Technology Conference, pp. 1–11

31. Brito R, Pereyra E, Sarica C (2014) Experimental study to characterize slug flow for medium oil viscosities in horizontal pipes. In 9th North American Conference on Multiphase Technology, pp. 403–417

32. Beggs DH, Brill JP (1973) A study of two-phase flow in inclined pipes. J Pet Technol 25(5):607–617

33. Khaledi H, Smith IE, Unander TE, Nossen J (2014) Investigation of two-phase flow pattern, liquid holdup and pressure drop in viscous oil–gas flow. Int J Multiphase Flow 67:37–51

34. Pan J (2010) Gas entrainment in two-phase gas-liquid slug flow. PhD Thesis, Imperial College London

35. Liu L, Hu B, Langsholt M, Yang Z (2014) Characteristics of gas-viscous oil flows in a 0.1 M diameter pipeline measured by an X-ray CT system. In 9th North American Conference on Multiphase Technology

36. Bestion D (1990) The physical closure laws in the CATHARE code. Nucl Eng Des 124(3):229–245

37. Choi J, Pereyra E, Sarica C, Park C, Kang J (2012) An efficient drift-flux closure relationship to estimate liquid holdups of gas-liquid two-phase flow in pipes. Energies 5(12):5294–5306

38. Zuber N, Findlay JA (1965) Average volumetric concentration in two-phase flow systems. J Heat Transf 87(4):453–468

39. Archibong-Eso A, Van W, Baba Y, Kanshio S, Yeung H (2015) Viscous liquid-gas flow in horizontal pipelines: Experiments and multiphase flow simulator assessment. In BHR Group - 17th International Conference on Multiphase Technology 2015

40. Colmenares J, Ortega P, Padrino J, Trallero JLL (2001) Slug flow model for the prediction of pressure drop for high viscosity oils in a horizontal pipeline. In Proceedings of SPE International Thermal Operations and Heavy Oil Symposium

41. Kora C, Sarica C, Zhang H, Al-Sarkhi A, Al-Safran E (2011) Effects of high oil viscosity on slug liquid holdup in horizontal pipes. In Canadian Unconventional Resources Conference

42. Gomez L, Shoham O, Taitel Y (Mar. 2000) Prediction of slug liquid holdup: horizontal to upward vertical flow. Int J Multiphase Flow 26(3):517–521

43. Al-Safran E (2009) Prediction of slug liquid holdup in horizontal pipes. J Energy Resour Technol 131(2):23001

44. Gregory GA, Nicholson MK, Aziz K (1978) Correlation of the liquid volume fraction in the slug for horizontal gas-liquid slug flow. Int J Multiphase Flow 4(1):33–39

45. Malnes D (1983) Slug flow in vertical, horizontal and inclined pipes. Institute for Energy Technology, Norway

46. Abdul-Majeed GH (2000) Liquid slug holdup in horizontal and slightly inclined two-phase slug flow. J Pet Sci Eng 27(1–2):27–32